Nanoscale

PAPER

View Article Online
View Journal | View Issue

Cite this: *Nanoscale*, 2021, **13**, 12602

Avidity and surface mobility in multivalent ligand–receptor binding†

Simon Merminod, ‡[a] John R. Edison, §[b] Huang Fang, [a] Michael F. Hagan [a] and W. Benjamin Rogers *[a]

Targeted drug delivery relies on two physical processes: the selective binding of a therapeutic particle to receptors on a specific cell membrane, followed by transport of the particle across the membrane. In this article, we address some of the challenges in controlling the thermodynamics and dynamics of these two processes by combining a simple experimental system with a statistical mechanical model. Specifically, we characterize and model multivalent ligand–receptor binding between colloidal particles and fluid lipid bilayers, as well as the surface mobility of membrane-bound particles. We show that the mobility of the receptors within the fluid membrane is key to both the thermodynamics and dynamics of binding. First, we find that the particle-membrane binding free energy—or avidity—is a strongly nonlinear function of the ligand–receptor affinity. We attribute the nonlinearity to a combination of multivalency and recruitment of fluid receptors to the binding site. Our results also suggest that partial wrapping of the bound particles by the membrane enhances avidity further. Second, we demonstrate that the lateral mobility of membrane-bound particles is also strongly influenced by the recruitment of receptors. Specifically, we find that the lateral diffusion coefficient of a membrane-bound particle is dominated by the hydrodynamic drag against the aggregate of receptors within the membrane. These results provide one of the first direct validations of the working theoretical framework for multivalent interactions. They also highlight that the fluidity and elasticity of the membrane are as important as the ligand–receptor affinity in determining the binding and transport of small particles attached to membranes.

Received 2nd April 2021,
Accepted 16th June 2021

DOI: 10.1039/d1nr02083h

rsc.li/nanoscale

Achieving the targeted binding of small particles to cell membranes has the potential to improve strategies for drug delivery; yet designing such interactions is challenging because the interactions are multivalent and the membranes are fluid and deformable. The basic idea is to coat a therapeutic payload with specific molecular species that bind it selectively—ideally exclusively—to cells of a specific identity, thereby maximizing a drug's efficacy while minimizing toxic side effects.[1–5] Achieving targeted binding thus requires the ability to design or select ligands that can recognize the biochemical attributes of the target cell without also binding to off-target membranes. This task is challenging because cell membranes comprise complex collections of various receptors with different concentrations depending on the cell's identity and health.[6] What is the optimal strategy for picking out one membrane composition over all the rest? Answering this question is complicated by the fact that the interactions between particles and membranes are typically multivalent—multiple pairs of ligands and receptors interact simultaneously—and the receptors in cell membranes are typically mobile and can diffuse on the membrane surface[7–9] (Fig. 1A). Therefore, while chemical complementarity ensures specific recognition between individual ligands and receptors, the selectivity of the binding response to molecular recognition is much more complex.

Simple *in vitro* systems and theoretical models provide a path toward a better fundamental understanding of multivalent interactions and how to design them. Qualitatively, the strength and specificity of multivalent interactions result from a subtle balance between enthalpy and entropy.[10] In the last decade, much progress has been made in developing theoretical models to predict multivalent interactions by combining

[a]*Martin A. Fisher School of Physics, Brandeis University, Waltham, MA 02453, USA. E-mail: wrogers@brandeis.edu*

[b]*Brandeis Materials Research Science and Engineering Center, Brandeis University, Waltham, MA 02453, USA*

† Electronic supplementary information (ESI) available: Text and figures about the DNA constructs, the colloidal particle synthesis and ligand grafting, the sample preparation, fluorescence recovery after photobleaching, the optical setup, the calibration of the total internal reflection microscope, the interaction potentials, the avidity, the theory of multivalent ligand–receptor binding, our model and numerical scheme, receptor recruitment, particle wrapping by the membrane, and the mobility of membrane-bound particles. See DOI: 10.1039/D1NR02083H

‡ Present address: Department of Molecular and Cellular Biology, Harvard University, Cambridge, MA 02138, USA.

§ Present address: Department of Chemical and Biomolecular Engineering, Johns Hopkins University, Baltimore, MD 21218, USA.

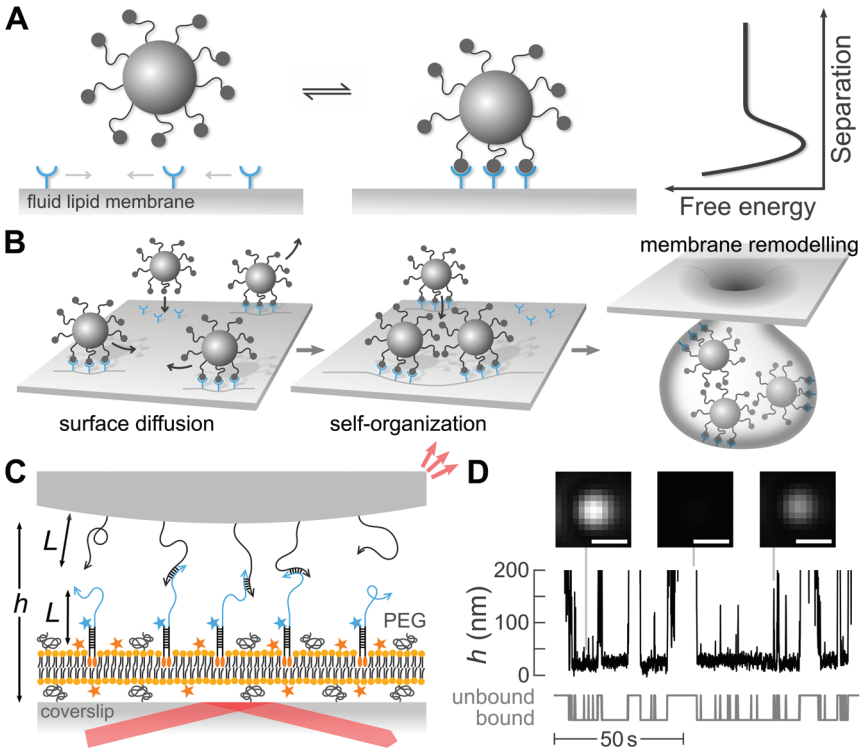

Fig. 1 Overview of the coupled physical processes that we study and of our experimental system. (A) Transient, multivalent ligand–receptor binding gives rise to an effective interaction potential between a colloidal particle and a fluid lipid membrane. How does the interaction potential depend on the ligand–receptor affinity, as well as the fluidity and elasticity of the membrane? (B) The lateral mobility of membrane-bound particles can enable membrane remodelling and cellular uptake. How does the mobility depend on the details of the particle-membrane interactions? (C) In our experimental system, DNA ligands grafted to a 1.4 μm-diameter colloidal particle hybridize with DNA receptors embedded in a supported lipid bilayer (SLB) to induce attractive interactions. Single-stranded DNA ligands and receptors have a typical length $L \approx 15$ nm. DNA receptors are labelled with 6-FAM fluorophores (blue stars) and anchored in the membrane using double cholesterol-triethylene glycol (TEG) modifications (orange ovals). The SLB is formed of a mixture of three phospholipid species, including 2.4% (w/w) that are labelled with Texas Red fluorophores (orange stars) and 0.5% (w/w) that are PEGylated (black coils). The particle scatters light (small red arrows) from an evanescent wave generated by a reflected laser beam (large red arrow). (D) The inferred colloid-glass separation, h, shows intermittent binding. A colloid is considered bound when h is smaller than a threshold value, roughly 45 nm. Insets show micrographs of the light scattered by the single colloidal particle at different moments along the trajectory. Bright spots correspond to small separations. Scale bars, 1 μm.

the tools of statistical physics with other system-specific frameworks, such as theories of membrane mechanics. This approach has been applied to situations in which the ligands and receptors are fixed[11,12] or mobile,[13] and the interfaces are rigid or deformable.[14–16] However, experimental validations of these various models lag behind.[16] While a few recent experimental studies have explored the physical mechanisms underlying the kinetics of binding, the membrane deformation due to multivalent interactions, or the factors influencing binding selectivity,[14,17–22] they do not measure the particle-membrane binding free energy (Fig. 1A). Therefore, direct experimental measurements of the binding free energy are needed to first validate, and then design, specific interactions between particles and membranes.

In addition to specific binding, the lateral mobility of membrane-bound particles also plays a major role in the transport of a therapeutic payload across a membrane. While a single bound particle whose adhesion energy is large compared with the bending rigidity of the membrane might be able to cross the membrane alone, by becoming fully wrapped by the membrane, more weakly bound particles cannot.[23] Instead, multiple weakly bound particles have to first self-organize *via* lateral attractions[24–27] to trigger remodelling of the membrane, such as collective budding[25,28,29] (Fig. 1B), in order to enter the cell. The success—or failure—of such processes hinges on surface mobility: for weakly bound particles to self-organize, they must find one another and sample configurations within their energy landscape faster than they unbind from the membrane. Thus, to engineer successful strategies for targeted delivery, we also need to understand how the lateral mobility of membrane-bound particles depends on the details of ligand–receptor binding.

In this article, we combine experiments and theory to characterize the relationships between the ligand–receptor affinity, the binding avidity, and the lateral mobility of colloidal particles interacting with supported bilayer membranes. We use complementary single-stranded DNA molecules as model ligand–receptor pairs, and measure the emergent interactions using total internal reflection microscopy. Using DNA

as ligands and receptors is crucial since it enables us to precisely tune the affinity *in situ* by adjusting the temperature. We find that the mobility of the receptors within the membrane plays a key role in determining both the avidity and the particle mobility, highlighting the importance of membrane fluidity in targeted delivery. Specifically, we find that the avidity is a strongly nonlinear function of the ligand–receptor affinity. A statistical mechanical model of the interactions shows that this nonlinear dependence results from a combination of multivalency and recruitment of receptors to the site of contact between the particle and the membrane. Disagreements between our measurements and model predictions in the limit of strong binding suggest that elastic membrane deformations further enhance the nonlinearity of avidity, by bending the membrane to increase the area of contact between the particle and the membrane. Combining measurements of the lateral diffusion of membrane-bound particles with predictions of the number and spatial distribution of bound receptors, we also show that the diffusion coefficient of membrane-bound particles is determined by the hydrodynamic drag against the aggregate of recruited receptors, and not by the viscosity of the surrounding solution. Taken together, our results show that the avidity and surface mobility of particles interacting with fluid membranes—two key ingredients in targeted delivery—are related through the mobility of the receptors. Therefore, our findings suggest that future attempts to design interactions to target specific cell membranes should consider the membrane fluidity and elasticity, in addition to the composition of receptors expressed on the membrane surface.

Results and discussion

Our experimental system consists of DNA-coated colloidal particles and DNA-functionalized supported lipid bilayers (SLBs). The particles are 1.4 μm-diameter spheres made of 3-(trimethoxysilyl) propyl methacrylate (TPM), which are coated with single-stranded DNA oligomers using click chemistry[30] (Fig. 1C). The supported lipid bilayers are comprised of 97.1% (w/w) 1,2-dioleoyl-*sn-glycero*-3-phosphocholine (18 : 1 DOPC), 2.4% (w/w) PEG(2k)-labeled 1,2-dioleoyl-*sn-glycero*-3-phosphoethanolamine (18 : 1 PE), and 0.5% (w/w) Texas Red-labeled 1,2-dihexadecanoyl-*sn-glycero*-3-phosphoethanolamine (DHPE). We make the supported bilayers by spreading liposomes on a cleaned glass coverslip. After spreading, we label the supported bilayer with DNA using a double-stranded DNA handle modified with two cholesterol molecules. One of the DNA handles is also modified with the fluorophore FAM. The PEGylated lipids ensure mobility of the receptors within the supported bilayer and prevent nonspecific binding of the particles to the membrane. The Texas Red-labeled lipids and FAM-labeled DNA molecules allow us to image the SLB and its DNA coating, and measure their fluidity. We verify that the lipids and surface-anchored DNA strands are mobile using fluorescence recovery after photobleaching (FRAP). See Materials and methods, as well as the ESI† for further details.

We measure the interactions and the lateral diffusion of colloidal particles from their three-dimensional trajectories, using total internal reflection microscopy. Briefly, a laser beam totally internally reflected from a glass–water interface creates an evanescent wave in the sample chamber (Fig. 1C). A colloidal particle within the evanescent wave scatters an amount of light that decreases exponentially with the separation between the particle and the coverslip, h.[31] We image the scattered light onto a sCMOS camera and quantify the scattered intensity, $I(t)$, using existing particle-tracking routines.[32] Using a calibration based on the hydrodynamic coupling of a sphere and a flat interface,[31,33] we infer the vertical position of the particle as a function of time, $h(t)$, from the scattered intensity, $I(t)$. We record videos at 100 Hz for a duration of 500 s, and image an average of 5 particles simultaneously. See the ESI† for a detailed description of the experimental setup and the calibration method.

Emergent colloidal-membrane interactions

Experimental measurements. We infer the colloid-membrane interaction potentials from the separation time series for each particle. Fig. 1D shows an example time series, in which the particle intermittently binds to and unbinds from the supported bilayer. Assuming that the particle is in thermal equilibrium, the distribution of its vertical separation h obeys Boltzmann statistics. Therefore, we measure the interaction potential between the particle and the membrane, $\Delta F_{\mathrm{tot}}(h)$, up to a constant by creating a histogram of the separations, $P(h)$, and then inverting the Boltzmann distribution, $P(h) \propto \exp[-\Delta F_{\mathrm{tot}}(h)/k_{\mathrm{B}}T]$, where k_{B} is the Boltzmann constant and T is the temperature. Finally, we subtract the linear contribution to $\Delta F_{\mathrm{tot}}(h)$ due to gravity to obtain the DNA-mediated interaction potentials, $\Delta F(h)$. We measure $\Delta F(h)$ for a number of different temperatures and three different receptor densities.

The interaction potentials that we measure feature a short-range attractive well whose depth depends sensitively on temperature. Fig. 2A–C show examples of interaction potentials for three different temperatures. All interaction potentials show a very short-range repulsion and a short-range attraction, with a well depth that increases with decreasing temperature. The range of the attractive wells spans roughly 20–30 nm above the membrane, which is comparable to twice the end-to-end distance of the grafted DNA molecules.[34]

We compute the avidity, ΔG_{av} for each interaction potential. Whereas the affinity tells us about the free energy of binding between a single ligand–receptor pair, the avidity tells us about the free energy of binding between the particle and membrane, which in general involves the cooperative interactions between many ligands and receptors. To account for both the range and depth of the attractive well, we define avidity from the integral of the Boltzmann weights over the bound state,[35,36]

$$\Delta G_{\mathrm{av}} = -k_{\mathrm{B}}T \log \left[(c_0 N_{\mathrm{A}})^{1/3} \int_0^{\lambda_{\mathrm{b}}} \mathrm{e}^{-\Delta F(h)/k_{\mathrm{B}}T} \mathrm{d}h \right], \qquad (1)$$

where c_0 = 1 mol l^{-1} is a reference concentration, N_{A} is Avogadro's number, and λ_{b} is the maximum separation within

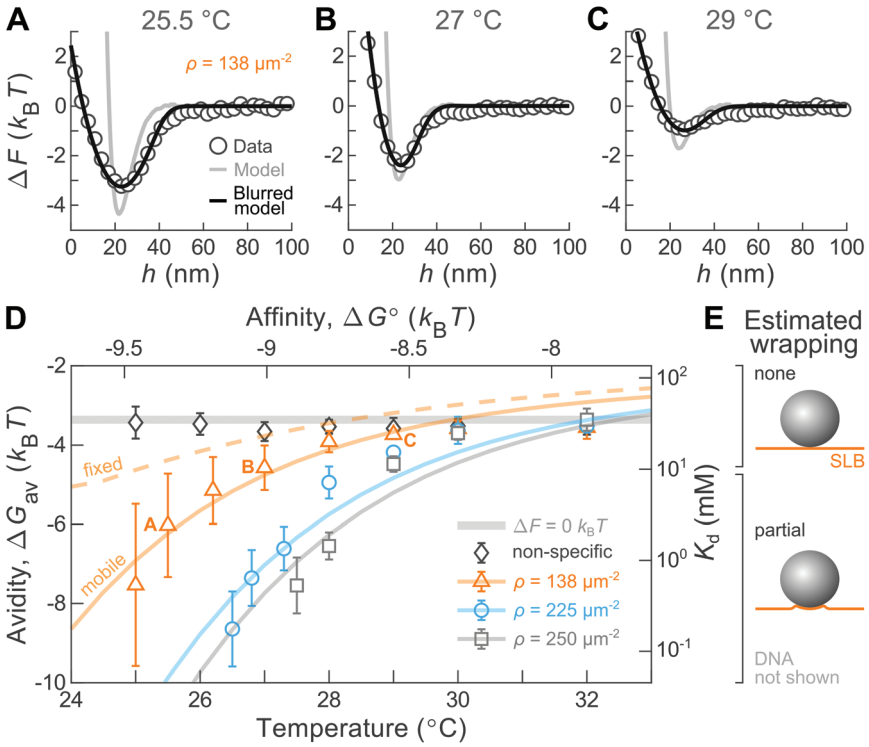

Fig. 2 Colloid-membrane interactions. (A–C) Example interaction potentials at fixed receptor density ρ = 138 μm^{-2} and increasing temperature show a temperature-dependent attractive well for T = 25.5 °C (A), 27 °C (B), and 29 °C (C). Circles are experimental data. Gray curves are the model; black curves are the model after blurring to account for the finite precision of our measurements. (D) The avidity, ΔG_{av}, defined in the text (eqn (1)), as a function of temperature and affinity, $\Delta G°$, for three receptor densities: ρ = 138 μm^{-2} (orange), ρ = 225 μm^{-2} (blue), and ρ = 250 μm^{-2} (gray). Experimental measurements (symbols) show that avidity is a strongly non-linear function of temperature. Solid curves are best-fit model predictions at fixed receptor density. Error bars denote the standard deviation of avidities measured for multiple particles. Annotations "A", "B", and "C" correspond to the conditions of panels A, B, and C. The dashed orange curve shows avidity from a model with fixed receptors, in contrast to the solid orange curve which shows predictions with mobile receptors. Experimental measurements of particles coated with noncomplementary ligands (diamonds) show a weak temperature-independent, nonspecific attraction. The thick gray curve shows the avidity for $\Delta F(h) = 0$ for all separations. The right axis shows the dissociation constant, $K_d = c_0 e^{\Delta G_{av}/k_B T}$, with c_0 = 1 mol l^{-1}. (E) We estimate that partial wrapping of the particle by the membrane occurs for avidities stronger than $-4.7 k_B T$, or K_d < 10 mM.

which ligands and receptors can bind. We set λ_b = 34 nm for all calculations (see the ESI† for details). Finally, we note that while avidity is a negative number, throughout the discussion, we use "increasing avidity" to mean a more negative value of avidity, and thus stronger binding.

We find that the avidity is a strongly nonlinear function of temperature, and increases with receptor density. Fig. 2D shows the experimentally measured avidities as a function of temperature for three receptor densities. In all three cases, the avidity decreases upon increasing temperature and increases with increasing receptor density. Furthermore, the avidity becomes a sharper function of temperature upon increasing receptor density, decreasing from $-8k_BT$ to $-3.5k_BT$ over roughly five degrees Celsius at the highest density. The thick gray line in Fig. 2D is the avidity for a system with $\Delta F = 0$ over the entire binding region, namely $\Delta G_{av} = -k_B T \log[\lambda_b (c_0 N_A)^{1/3}]$, which arises from the probability of particles residing within the binding volume even in the absence of interactions. Control experiments using particles grafted with noncomplementary DNA sequences yield an avidity of roughly $-3.5k_BT$ at all temperatures. While this value is close to the avidity for $\Delta F = 0$, we note that particles are excluded from the region of small separation, $h \lesssim 20$ nm, and thus this value implies a weak attraction for separations between 20 nm and λ_b. We speculate that this weak nonspecific attraction results from nonspecific interactions between the TPM particles and the PEG molecules grafted to the membrane. Finally, although we present our experimental findings in terms of their relationship to the temperature, we note that the key physical quantity is actually the ligand–receptor affinity, which itself is a linear function of the temperature.[37]

These qualitative relationships between avidity, affinity, and receptor density are consistent with physical intuition—greater affinity and larger receptor densities favor the formation of ligand–receptor bonds. However, unpacking the emergent interactions further requires a theoretical model. In the following, we use a statistical mechanical model and compare its predictions to our experimental measurements. The advantage of such a microscopic model is that it allows us to dissect the relevant contributors to the avidity, such as multivalency,

receptor mobility, and even elastic membrane deformations. Which of these effects are dominant? And how do they alter the relationship between affinity and avidity?

Theoretical model. The emergent interactions between two surfaces decorated with DNA molecules arise from a rich interplay of enthalpic and entropic effects. When the surfaces are close enough, complementary strands can hybridize to form bridges by Watson–Crick base pairing, lowering the enthalpy of the system. However, when two complementary strands bind, they must also incur a distance-dependent entropic penalty, as they sacrifice degrees of freedom in order to hybridize. Even the unhybridized ligands and receptors can lose configurational entropy when they are squeezed between the two surfaces, an effect which again depends on the separation distance. Finally, the mobility of the membrane-anchored receptors complicates the situation further, since the mobile receptors can enrich or deplete the confined region between the particle and the membrane by paying an associated cost in mixing entropy.[16]

We model the particle-membrane interactions using a statistical mechanical theory of multivalent interactions developed by Mognetti, Frenkel, and coworkers.[11,16] We model the ligands and receptors as ideal chains with sticky ends, and the SLB as a flat plate in contact with a grand canonical reservoir of receptors. Details about the theoretical framework, the relevance of this framework to our experiments given the timescales in our system, and our semi-analytical approach to estimate the effective particle-membrane interactions are in the ESI.† All of the model parameters are constrained by experimental measurements with the exception of the receptor grafting density, ρ, which we choose to obtain the best match between the modeled and experimentally measured avidities (see the ESI†).

Comparing experiments and theory. Predictions from our model reproduce many aspects of our experimental measurements, with the receptor density as the only adjustable parameter. For the lowest receptor density, predictions of the avidity closely match our experimental measurements (Fig. 2D). Furthermore, the modeled interaction potentials—convolved with a Gaussian kernel to simulate the finite precision of our measurements—reproduce the full shape of the experimental potentials (Fig. 2A–C). For the two larger densities, the model also agrees well with experimental results, although not as closely as for the lowest density. The only significant disagreement between theory and experiment is the extent of the nonlinearity of avidity with respect to temperature: the avidity increases more sharply upon decreasing temperature in the experiments as compared to the model. Another minor disparity concerns the value of the plateau of avidity at high temperatures, which is lower in the experiments than in the model. This disparity arises because the experimental potentials have a small attractive well from non-specific attraction even at the highest temperatures, while the simulated potentials do not.

Importantly, the best-fit receptor densities that we find are consistent with our experimental conditions. The values range from roughly 130–250 molecules per μm^2, corresponding to an average spacing between receptors of about 60–90 nm. These typical distances are not so small as to be incompatible with the spontaneous adsorption of receptors to the membrane. They are also not so large as to prevent the formation of multiple ligand–receptor pairs between the particle and the membrane in a reasonable amount of time. Thus the receptor densities fall within a range that is consistent with both spontaneous adsorption and multivalent binding. Finally, we note that the fitted receptor densities are all smaller than the ligand density, which is roughly 1200 ligands per μm^2. As a result, there are many more ligands than receptors in the gap between a particle and the membrane, which can drive recruitment of fluid receptors during binding.

We hypothesize that elastic membrane deformations—which we do not model here—explain the disagreement between theory and experiment at low temperatures. Because fluid membranes are elastic, they can deform upon binding of a particle. As shown by Deserno,[23] and recently verified for nanoparticles binding to lipid vesicles,[29] one can predict the onset of such deformations in free membranes from the dimensionless ratio $\tilde{w} = 2wa^2/\kappa$, where w is the particle-membrane adhesion energy per unit area, a is the radius of the adhering particle, and κ is the membrane bending rigidity. Taking σ to be the membrane tension and defining $\tilde{\sigma} = \sigma a^2/\kappa$, the theory predicts that the membrane will remain flat when $\tilde{w} < 4$, undergo small deformations and partial particle wrapping when $4 < \tilde{w} < 4 + 2\tilde{\sigma}$, and fully wrap the particle when $\tilde{w} > 4 + 2\tilde{\sigma}$. Taking typical values for DOPC supported bilayers —$\sigma = 1$ pN nm^{-1} and $\kappa = 20k_BT$[29,38]—we estimate that $\tilde{\sigma} \approx 6000$ and $\tilde{w} \approx 1$–9 over our range of avidities. More specifically, we expect the membrane to remain undeformed in our system when the avidity is smaller than $-4.7k_BT$, and partially wrap the particles at stronger avidities (Fig. 2E and more details in the ESI†).

Our measurements of avidity agree with these expectations of membrane deformation. For the two largest receptor densities, we observe that the avidity is a steeper function of temperature below about $-5k_BT$, which is roughly equal to our estimate of the onset of membrane bending of $-4.7k_BT$ (Fig. 2D and E). Even though the model by Deserno concerns free—not supported—membranes,[23] we believe that it is relevant to the present discussion because the membrane deformations are likely smaller than the size of our PEG spacers, which separate the membrane from the glass substrate by roughly 3 nm.[39] In fact, for the largest avidity that we measure, roughly $-9k_BT$, we estimate that the patch of deformed membrane has a diameter of roughly 40 nm, and a deflection of only 0.5 nm above the flat membrane.[23] Unfortunately, we do not have the resolution to confirm this prediction. Finally, we suspect that membrane mechanics are modified by the addition of the DNA receptors. In fact, we observe various membrane instabilities upon the addition of receptors, such as the spontaneous formation of tubules extending tens of micrometers into the bulk. These observations indicate that the bound receptors might facilitate membrane deformation, which is consistent with our observation that the disagreement between theory and experiment is more pronounced for the higher receptor densities.

Contributions to avidity from multivalency and mobility. Digging further into the model, we find that both the multivalency of binding and the mobility of receptors within the fluid membrane contribute to the nonlinearity in avidity. If the interactions were monovalent, the avidity would be a linear function of affinity. Therefore, the nonlinear dependence of avidity that we observe reflects the cooperative nature of the simultaneous interactions of many ligand–receptor pairs. We isolate the effect of multivalency by computing the avidity in a variation of our usual system—a simulated system in which receptors are anchored at specific points on the membrane—but is otherwise identical to our system with mobile receptors. In particular, the receptor grafting density in the fixed system is equal to the receptor density within the grand canonical reservoir in the mobile system, ρ. The difference in avidity between these two systems is thus due to receptor mobility. We compute the avidity in the fixed system for a single receptor density of 138 μm^{-2}. The avidity that we obtain is again a nonlinear function of affinity, but exhibits a weaker dependence on temperature than both our experimental measurements and our predictions within the mobile system (Fig. 2D). Thus, multivalency is only one piece of the puzzle.

Our theoretical model reveals that recruitment of receptors to the binding site—due to their mobility—is responsible for the remaining nonlinearity in the avidity. We confirm this physical picture by computing the excess number of receptors within the gap as a function of the temperature for three receptor densities (Fig. 3A). We find that the number of excess receptors is always positive; thus, mobile receptors are always recruited on average (illustrated in Fig. 3B). We also find that the excess number of receptors, and thus the extent of recruitment, is larger at lower temperatures. In other words, as the ligand–receptor affinity increases, more receptors can overcome the entropic cost required to enrich the gap between the particle and the membrane. It is precisely this coupling between the ligand–receptor affinity and the entropy penalties of recruiting and confining the receptors in the gap that further enhances the avidity at lower temperatures. Finally, we note that more receptors are recruited at larger receptor densities and that the number of excess receptors does not plateau at low temperatures, indicating that the ligands grafted to the particles are not saturated by the receptors within the range of receptor densities that we explore. See the ESI† for more details on receptor recruitment.

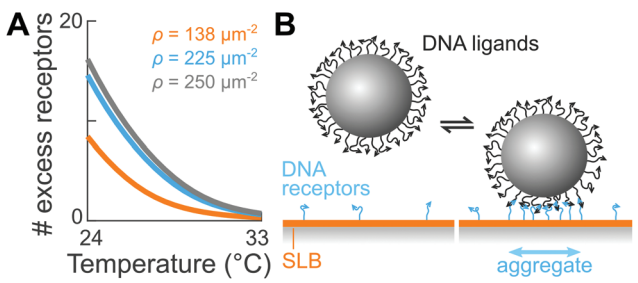

Fig. 3 Receptor recruitment. (A) Model predictions of the excess number of receptors in the gap between the particle and the supported bilayer as a function of temperature for three receptor densities, showing that receptors are recruited upon binding, and that recruitment is stronger at lower temperatures and larger receptor densities. (B) Schematics illustrating receptor recruitment.

In this section, we showed how the unique combination of DNA as a model ligand–receptor pair, total internal reflection microscopy, and statistical mechanics can shed light on the molecular-scale mechanisms governing adhesion between small particles and membranes. Beyond the effects of multivalency alone, our experiments and model demonstrate that the recruitment of receptors, as well as particle wrapping, play essential roles in determining the avidity of binding, and thus need to be accounted for when designing particles for targeted binding to cell membranes. These observations constitute one of the first direct experimental validations of the theoretical framework by Mognetti, Frenkel, and coworkers.[11,16]

Surface mobility

Whereas the discussion above focused on the thermodynamics of adhesion between colloidal particles and fluid bilayer membranes, targeted delivery could also be influenced by the mobility of adhered particles on the membrane surface, for instance to collectively remodel the membrane.[25,28,29] In this section, we determine the relationship between the surface mobility of bound colloids and the physical properties of their receptor aggregates, as well as the avidity.

We characterize the lateral mobility of membrane-bound particles from their three-dimensional trajectories. First, we segment each trajectory into bound and unbound events by setting a threshold separation h_b (see the ESI† for details and Fig. 1D for an example). Within each bound event, we then compute the two-dimensional mean squared displacement (MSD) as a function of lag time. Finally, we extract a diffusion coefficient, D, for each particle by fitting the average of the mean squared displacement over all bound events to MSD = $4Dt$, where t is the lag time.

The membrane-bound particles undergo Brownian diffusion and have mobilities that are strongly correlated with both temperature and receptor density. Fig. 4A shows representative MSDs at the lowest receptor density for a range of temperatures. All MSDs grow linearly with time, indicating Brownian diffusion. The MSDs are truncated at the highest temperatures due to the short bound lifetimes. Fig. 4B shows the diffusion coefficients for every particle we studied. For a given grafting density, the diffusion coefficient D increases by a factor of roughly two upon increasing temperature over the full range. Additionally, the diffusion coefficient D is smaller than—or within the estimated range of—the diffusion coefficient expected for colloids diffusing freely between 5–50 nm above the membrane,[40] which suggests that binding hinders surface mobility.

Furthermore, increasing receptor density decreases the diffusion coefficient D at fixed temperature, suggesting again that adhesion plays a significant role in determining the mobility of membrane-bound particles. Indeed, rescaling the diffusion coefficient by the binding avidity collapses all of our

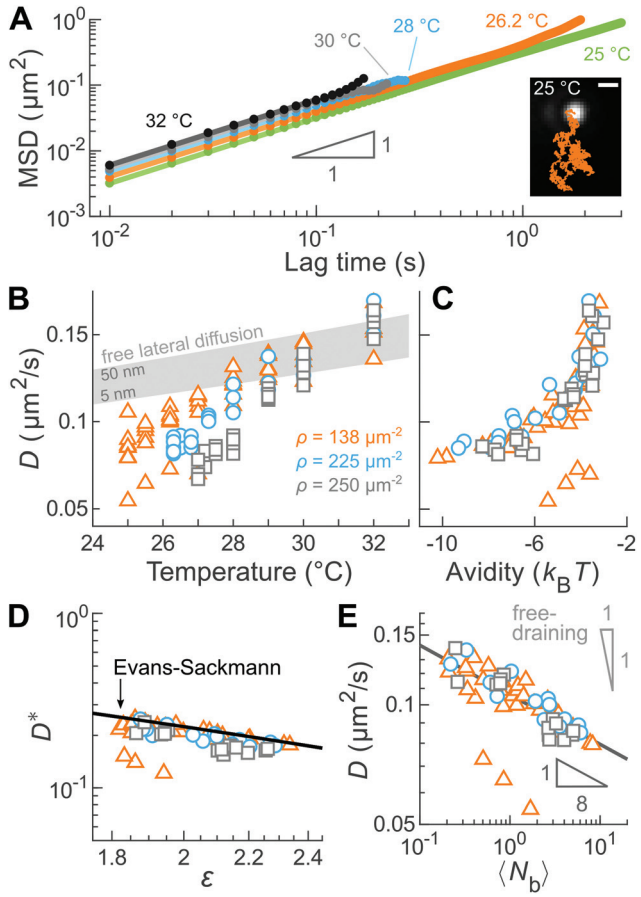

Fig. 4 Mobility of membrane-bound particles. (A) Experimental measurements (circles) of the mean-squared displacements (MSD) as a function of lag time, t, and their linear fits of MSD = $4Dt$ (lines), where D is the coefficient of diffusion, for selected temperatures at a fixed density ρ = 138 μm^{-2}. The inset shows a two-dimensional trajectory of a single particle (orange) overlayed on a micrograph of the last frame of the trajectory. Scale bar, 1 μm. The deviations from a slope of one at the longest lag times are a result of poor sampling. (B) Measurements of the diffusion coefficient (symbols) of membrane-bound particles as a function of temperature for three receptor densities. The shaded area indicates the range of diffusion coefficients expected for freely diffusing colloids between 5–50 nm above the membrane.[40] (C) Measurements of D (symbols) as a function of avidity for three receptor densities collapse to a single curve, demonstrating the coupling between the binding avidity and the latteral mobility. (D) The Evans–Sackmann model[41] quantitatively predicts our measurements. D^* is a dimensionless diffusion coefficient and ε is a dimensionless aggregate radius, defined in the main text. Symbols show calculated values of D^* and ε from experimental measurements. The black solid curve shows predictions of the Evans–Sackmann model with no adjustable parameters. (E) In contrast, the free-draining model fails to describe our measurements. Points show measurements of D with respect to the average number of bonds $\langle N_b \rangle$. The data collapses to a power law with an exponent of roughly −1/8 (solid line). Physical parameters for the models are the membrane viscosity, η_m = 0.14–0.19 Pa s, the bulk viscosity, η_b = 0.80–0.93 mPa s, the membrane thickness, h_m = 3.8 nm, and the glass-membrane separation, H = 3.1 nm.

experimental measurements to a single curve (Fig. 4C), suggesting that the avidity is the essential physical variable governing mobility.

To elucidate the physical origin of this coupling, we hypothesize that the lateral mobility of membrane-bound particles is dictated by the mobility of their receptor aggregates within the bilayer membrane. To explore the relationship between ligand–receptor binding and surface mobility, we compare our experimental measurements to two classical models: (1) a model from Evans and Sackmann;[41] and (2) the free-draining model.[17,42–44] These two models differ in how they compute the hydrodynamic drag on an inclusion diffusing within a fluid membrane. In our system, we take the inclusion to be the aggregate of cholesterol molecules that tether the receptors to the lipid membrane. The free-draining model assumes that the inclusion is permeable to lipids and unbound receptors, such that the total drag on the inclusion is simply the sum of the drag against each cholesterol anchor, leading to:

$$D \propto \langle N_b \rangle^{-1}, \tag{2}$$

where $\langle N_b \rangle$ is the average number of ligand–receptor bonds.[17,42–44] In the opposite limit, the inclusion is completely impermeable and diffuses like a single, unit aggregate. Saffman and Delbrück first predicted the diffusion coefficient D from the aggregate radius, R, for free membranes.[45] This model was later extended by Evans and Sackmann for the case of supported lipid bilayers to account for the hydrodynamic interactions between the membrane constituents—both the lipids and the aggregate—and the support.[41] The Evans–Sackmann model predicts:

$$D = \frac{k_B T}{4\pi\eta_m h_m}\left[\frac{\varepsilon^2}{4}\left(1+\frac{b_p}{b_s}\right)+\frac{\varepsilon K_1(\varepsilon)}{K_0(\varepsilon)}\right], \tag{3}$$

where η_m is the membrane viscosity, h_m is the membrane thickness, b_p is the inclusion-substrate coefficient of friction, b_s is the membrane-substrate coefficient of friction, and K_ν are the modified Bessel functions of the second kind. ε is a dimensionless aggregate radius:

$$\varepsilon \approx R\left(\frac{\eta_b}{H h_m \eta_m}\right)^{1/2}, \tag{4}$$

where η_b is the viscosity of the bulk fluid and H is the separation between the membrane and its substrate. This approximate form of ε is accurate in the limit of $H \ll L_{SD}$, where $L_{SD} = h_m\eta_m/2\eta_b$ is the Saffman-Delbrück length giving the range of hydrodynamic coupling between membrane inclusions.[46] In our experiments, H = 3.1 nm due to the PEGylated lipids and L_{SD} = 300–400 nm; hence the condition $H \ll L_{SD}$ is met. For simplicity, we assume $b_p = b_s$. See the ESI† for more details.

To test these two predictions, we rescale our measurements of the diffusion coefficient using a combination of experimental and theoretical results. Whereas we measure the diffusion coefficient, D, directly in our experiments, we cannot measure the average number of bridges in an aggregate, $\langle N_b \rangle$, nor the aggregate radius, R. Instead, we rely on predictions from our statistical mechanical model to infer these two quan-

tities from our measurements of the well depth of the interaction potentials. Specifically, we create phenomenological relationships between $\langle N_b \rangle$ and the well depth, and between R and the well depth using predictions from our model. We then use these one-to-one mappings to infer the average number of bridges and the aggregate radius from the measured interaction potentials (see the ESI†).

We find that the Evans–Sackmann model quantitatively describes our measurements of the mobility of membrane-bound particles. Defining a dimensionless diffusion coefficient, $D^* = D4\pi\eta_m h_m/k_B T$, which corresponds to the translational mobility of an inclusion within the membrane, we find that all of our experimental measurements of D^* collapse on a single curve when plotted as a function of the dimensionless aggregate radius ε (Fig. 4D). Moreover, plugging in the physical constants for our experimental system, we see that the Evans-Sackmann model quantitatively predicts both the trend and the magnitude of the dimensionless diffusion coefficient D^*. In contrast, the Saffman–Delbrück model[45,47,48] is off by roughly one order of magnitude, as shown in the ESI.† In retrospect, this result is unsurprising since the membranes in our experiments are supported on a glass substrate.

The validity of the Evans–Sackmann model is likely due to strong hydrodynamic coupling between the cholesterol anchors within the receptor aggregates. As mentioned above, the range of hydrodynamic coupling between membrane inclusions is given by the Saffman–Delbrück length, L_{SD}, which is roughly 300–400 nm in our experiments. By comparison, we estimate that the receptors within the aggregate are separated by only 40–80 nm. Because this estimate is one order of magnitude smaller than the Saffman–Delbrück length, we hypothesize that receptors are strongly coupled.

In contrast, the free-draining model does not reproduce our experimental observations. Replotting our measurements of the diffusion coefficient D against $\langle N_b \rangle$ collapses the data onto a single curve with a power-law exponent of $-1/8$ (Fig. 4E). While the collapse indicates that $\langle N_b \rangle$ is a relevant parameter in governing the lateral diffusion coefficient D, the $-1/8$ dependence that we find is much weaker than the -1 prediction of the free-draining model (eqn (2)). Interestingly, in a system sharing many similar features as our own, Block and collaborators found that the diffusion of lipid vesicles adhered to a supported bilayer by few, long-lived DNA bonds was accurately described by the free-draining model.[17] While we estimate that the typical distances between DNA bonds in their system and ours are comparable, other features—such as the fraction of PEGylated lipids and, possibly, the DNA receptor density—are not. In particular, the receptors in the studies by Block and coworkers were anchored to the membrane using cholesterol molecules, while we use cholesterol-triethylene glycol (TEG) modifications. Because the hydrophilic TEG groups enable the anchors to spontaneously insert deep into the lipid bilayer,[49,50] we hypothesize that the details of the hydrodynamic drag differ in the two cases.

Conclusions

We set out to elucidate the physical principles that determine the thermodynamics and dynamics of multivalent ligand–receptor binding between small particles and fluid membranes, with the ultimate goal of identifying the key players implicated in targeted drug delivery. Using a new experimental model system combining DNA-coated colloids with DNA-labeled lipid bilayers, we characterized and modeled adhesion, surface mobility, and their interplay in multivalent ligand–receptor binding. We showed that the strength of adhesion—or avidity—is a strongly nonlinear function of the affinity of the individual ligand–receptor pairs. This nonlinearity results from three contributions: (1) the statistical mechanics of multivalent binding; (2) the recruitment of mobile receptors embedded within the membrane; and (3) the adhesion-mediated elastic deformations of the membrane. We also found that membrane-bound particles undergo two-dimensional Brownian motion, with a mobility that is dictated by that of their aggregate of receptor anchors. Combining theoretical predictions with direct experimental measurements, we demonstrated that the mobility of a membrane-bound particle is accurately predicted by the Evans–Sackmann model of impermeable, solid inclusions diffusing in supported membranes. This result suggests a strong hydrodynamic coupling between the cholesterol molecules within the aggregate. Taken together, our study provides one of the first direct experimental validations of the theoretical framework developed by Mognetti, Frenkel, and coworkers[11,16] for a system with fixed ligands and mobile receptors—a configuration with direct relevance to targeted drug delivery.[8–10]

Going forward, our findings suggest that future approaches to designing targeted interactions between colloidal particles and fluid membranes should include the mobility of receptors and the deformability of the membrane, in addition to the specificity of ligand–receptor binding. As we hypothesize in this article, membrane deformations are important because they can occur for relatively weak interactions, yet produce a substantial increase in avidity. This enhancement is due to the large increase in contact area that can be generated by even small deformations. For instance, in our experimental system, we estimate that deformations of roughly 0.5 nm can increase avidity by roughly $1k_B T$, an amount that is comparable to the contributions from multivalency or receptor mobility. Therefore, we suggest that future models of targeted binding also determine the shape of the membrane by minimizing the elastic energy considering contributions from membrane bending and stretching,[51] in addition to the adhesion energy.[11,16] One such approach was recently implemented in a theoretical study of receptor-mediated endocytosis.[15]

Finally, we envision that our results and experimental approaches—mediating interactions using DNA ligand–receptor pairs—could be extended to control and study the self-assembly of colloidal particles bound to lipid vesicles. Self-assembly of nanometer-scale particles bound to fluid membranes, such as membrane proteins, is central to many biologi-

cal processes, including membrane trafficking, cell division, and cell movement.[52,53] Furthermore, the cooperative assembly and folding of membranes and membrane-bound proteins can also generate amazing nanostructured materials, like the structurally colored wing scales of many butterflies.[54] There, deformations of the membrane give rise to long-range elastic forces between inclusions that direct them to self-assemble. Could we recapitulate similar processes using colloids that bind to and deform membranes?[26,27] Using DNA to control the self-assembly of colloids on lipid vesicles could open new possibilities in programmable self-assembly. One unique feature of our DNA-based approach is that the adhesion energy can be tuned *in situ via* the temperature, and predicted using the model validated in this article. Moreover, one can even imagine studying self-assembly of multiple particle species with orthogonal ligand–receptor pairs, different particle sizes, different adhesion strengths, and thereby different degrees of wrapping. We anticipate that such multicomponent systems could produce a complex diversity of structures that far exceeds the types of structures that can be built from colloids or lipids alone.

Materials and methods

DNA-grafted particles

We synthesize 3-(trimethoxysilyl)propyl methacrylate (TPM) colloids using an emulsification technique.[30] The synthesized particles are 1.43 μm-diameter spheres and have a density of 1.228 g cm^{-3}.[55] We graft the TPM colloids with dibenzocyclooctyne-amine (DBCON)-modified single-stranded DNA molecules (Integrated DNA Technologies, Inc.) using click chemistry.[30] The particles are stored in aqueous buffer containing 10 mM Tris-HCl/1.0 mM EDTA/pH = 8.0.

DNA-grafted supported lipid bilayers

We make supported lipid bilayers (SLBs) by fusion of small unilamellar vesicles (SUVs) on a glass coverslip. This lipid mixture is composed of 97.1% (w/w) 1,2-dioleoyl-*sn-glycero*-3-phosphocholine (18 : 1 DOPC, Avanti Polar Lipids), 2.4% (w/w) 1,2-dioleoyl-*sn-glycero*-3-phosphoethanolamine-*N*-[methoxy(polyethylene glycol)-2000] (18 : 1 PEG2000 PE, Avanti Polar Lipids), and 0.5% (w/w) Texas Red 1,2-dihexadecanoyl-*sn-glycero*-3-phosphoethanolamine (Texas Red DHPE, Thermo Fisher Scientific). Briefly, we make SUV suspensions by overnight hydration of a dried lipid film followed by sonication. Since large vesicles scatter visible light while SUVs do not, we visually inspect the suspensions after sonication to make sure that they appear clear. SUV suspensions are stored in aqueous buffer containing 20% (v/v) glycerol/10 mM Tris-HCl/1.0 mM EDTA/pH = 8.0. We fabricate sample chambers with a combination of glass coverslips (VWR), Parafilm (Bemis Company, Inc.) and polydimethylsiloxane (PDMS, Sylgard 184, Dow). We incubate SUVs with chemically- and plasma-cleaned glass coverslips for 30 min to form the SLB and then wash out excess vesicles.

We functionalize the SLB with DNA receptors using a double cholesterol anchor. To tune the receptor density within the membrane, we adjust the receptor concentration and incubation time. Receptors are formed from two cholesterol-triethylene glycol (TEG)-modified single-stranded DNA molecules (Integrated DNA Technologies, Inc.) by thermal annealing. The short DNA strand is labeled with a 6-FAM fluorophore and the long DNA strand carries the sticky end. Hybridized receptors are stored in aqueous buffer containing 500 mM NaCl/10 mM Tris-HCl/1.0 mM EDTA/pH = 8.0.

We use a laser scanning confocal microscope (TCS SP8, Leica Microsystems GmbH) equipped with a 20x objective (non-immersion, HCX PL Fluotar, numerical aperture, NA = 0.50, Leica Microsystems GmbH) and photomultiplier tubes to visually inspect the SLB and to carry out fluorescence recovery after photobleaching experiments to confirm the mobility of the lipids (Texas Red channel, excitation wavelength 552 nm) and the receptors (6-FAM channel, excitation wavelength 488 nm).

DNA interactions

The DNA ligands and receptors hybridize *via* complementary sticky ends, 5′-TTTTTTCTCTTA-3′ and 5′-TTGTCCTAAGAG-3′, respectively. The underlined portions are the sticky ends which bind to form a 6-basepair duplex. Each sticky end is separated from the base of the strand by a poly-T spacer. We design these DNA sequences so that the particle-membrane binding strength is roughly $1–10 k_B T$ between 25–35 °C. Thermodynamic parameters are $\Delta H^\circ = -40.9$ kcal mol^{-1} and $\Delta S^\circ = -118.4$ cal K^{-1} mol^{-1}.[56,57]

Interaction potentials and membrane-bound particle mobility

We measure the DNA-mediated particle-membrane interactions and the lateral mobility of bound particles using a custom-made, prism-based total internal reflection microscope. We match the refractive index of the glass sample chamber to the prism (68°, N-BK7, Tower Optical Corp.) using immersion oil (type N, Nikon Corp.). We control the sample temperature using a thermoelectric module and a thermistor (TE Technology, Inc.) placed under and on top of the prism, respectively, and a custom-made water block. When a colloidal particle is in the evanescent wave, it scatters an amount of light which decreases exponentially with the particle-glass separation distance h.[31] Light scattered by the particles is imaged using an upright microscope consisting of a 40x non-immersion objective (infinity-corrected, Plan Fluor, numerical aperture, NA = 0.75, Nikon Corp.), a tube lens (focal length, 200 mm, ThorLabs) and a high-speed sCMOS camera (Zyla 5.5, Andor, Oxford Instruments) recording at roughly 100 frames per second. We measure the scattered intensity as a function of time[32] and then construct a histogram of particle-glass separations, h, from which we compute the particle-SLB interaction potential by inverting the Boltzmann distribution. We compute the mean squared displacement of membrane-bound particles during bound events, which we identify using a threshold on the separation h. All experiments were performed

in aqueous buffer containing 500 mM NaCl/10 mM Tris-HCl/1.0 mM EDTA/pH = 8.0.

Modeling the interactions

We use a semi-analytical approach based on the theoretical framework developed by Mognetti, Frenkel, and coworkers[11,16] to estimate the interactions between a colloidal particle and the membrane. We model the DNA ligands and receptors as ideal chains with 10 and 8 segments, respectively, and of a Kuhn length of 4 nm. First, we estimate the free energy between a pair of plates separated by a distance $\tilde{h}$. The grafting density of the upper plate matches that of the colloidal particles used in experiment. The lower plate is attached to a grand canonical reservoir to mimic the presence of mobile receptors in our system. The adhesion energy between the two plates is:

$$\beta F_{\mathrm{adh}}(\tilde{h}) = \rho A(1-\chi_{\mathrm{r}}) - N_{\mathrm{l}}\log\chi_{\mathrm{l}} - N_{\mathrm{l}}\log(1+\overline{N}_{\mathrm{r}}\Xi\chi_{\mathrm{r}}), \qquad (5)$$

where $\beta = 1/k_{\mathrm{B}}T$, ρ is the density of the grand canonical reservoir of receptors, A is the plate area, N_{l} is the number of ligands, $\overline{N}_{\mathrm{r}}$ is the number of recruited receptors, $\chi_{\mathrm{l/r}}$ is proportional to the reduction in degrees of freedom associated with confining an ideal chain between two plates, and Ξ is proportional to the confinement-dependent hybridization free energy. We use estimations of βF_{adh}, together with the Derjaguin approximation, to estimate the interaction potential between a DNA-grafted spherical particle and a lipid membrane bearing mobile DNA receptors. More details of our approach can be found in the ESI.†

Author contributions

S. M., J. R. E., M. F. H. and W. B. R. designed research; S. M., J. R. E., and H. F. performed research; all authors analyzed data and wrote the paper; W. B. R. is the corresponding author.

Conflicts of interest

There are no conflicts to declare.

Acknowledgements

We thank Tijana Ivanovic, Tian Li, Larry Friedman, and Thomas Fai for helpful discussions, Melissa Rinaldin for her comments on the manuscript, and Francisco Mello and Gregory Widberg for the design and fabrication of the cooling block. We acknowledge support from the National Science Foundation (DMR-1710112), the Brandeis MRSEC Bioinspired Soft Materials (DMR-1420382 and DMR-2011846), the National Institutes of Health (R01GM108021 from the National Institute Of General Medical Sciences), and the Smith Family Foundation. We acknowledge computational resources provided by NSF XSEDE (award number MCB090163) and the Brandeis HPCC which is partially supported by DMR-2011846.

References

1 Y. H. Bae and K. Park, *J. Controlled Release*, 2011, **153**, 198–205.
2 V. P. Torchilin, *Nat. Rev. Drug Discovery*, 2014, **13**, 813–827.
3 O. Veiseh, J. W. Gunn and M. Zhang, *Adv. Drug Delivery Rev.*, 2010, **62**, 284–304.
4 S. Wilhelm, A. J. Tavares, Q. Dai, S. Ohta, J. Audet, H. F. Dvorak and W. C. W. Chan, *Nat. Rev. Mater.*, 2016, **1**, 16014.
5 B. Mishra, B. B. Patel and S. Tiwari, *Nanomedicine*, 2010, **6**, 9–24.
6 B. Alberts, A. D. Johnson, J. Lewis, D. Morgan, M. Raff, K. Roberts and P. Walter, *Molecular Biology of the Cell*, Garland Science, New York, NY, 6th edn, 2015.
7 F. J. Martinez-Veracoechea and D. Frenkel, *Proc. Natl. Acad. Sci. U. S. A.*, 2011, **108**, 10963–10968.
8 T. Curk, J. Dobnikar and D. Frenkel, *Proc. Natl. Acad. Sci. U. S. A.*, 2017, **114**, 7210–7215.
9 C. B. Carlson, P. Mowery, R. M. Owen, E. C. Dykhuizen and L. L. Kiessling, *ACS Chem. Biol.*, 2007, **2**, 119–127.
10 M. Mammen, S.-K. Choi and G. M. Whitesides, *Angew. Chem., Int. Ed.*, 1998, **37**, 2754–2794.
11 P. Varilly, S. Angioletti-Uberti, B. M. Mognetti and D. Frenkel, *J. Chem. Phys.*, 2012, **137**, 094108.
12 S. Angioletti-Uberti, B. M. Mognetti and D. Frenkel, *Phys. Chem. Chem. Phys.*, 2016, **18**, 6373–6393.
13 S. Angioletti-Uberti, P. Varilly, B. M. Mognetti and D. Frenkel, *Phys. Rev. Lett.*, 2014, **113**, 128303.
14 S. F. Shimobayashi, B. M. Mognetti, L. Parolini, D. Orsi, P. Cicuta and L. Di Michele, *Phys. Chem. Chem. Phys.*, 2015, **17**, 15615–15628.
15 L. Di Michele, P. K. Jana and B. M. Mognetti, *Phys. Rev. E*, 2018, **98**, 032406.
16 B. M. Mognetti, P. Cicuta and L. Di Michele, *Rep. Prog. Phys.*, 2019, **82**, 116601.
17 S. Block, V. P. Zhdanov and F. Höök, *Nano Lett.*, 2016, **16**, 4382–4390.
18 L. Parolini, B. Mognetti, J. Kotar, E. Eiser, P. Cicuta and L. Di Michele, *Nat. Commun.*, 2015, **6**, 5948.
19 S. J. Bachmann, J. Kotar, L. Parolini, A. Šarić, P. Cicuta, L. Di Michele and B. M. Mognetti, *Soft Matter*, 2016, **12**, 7804–7817.
20 R. Lanfranco, P. K. Jana, L. Tunesi, P. Cicuta, B. M. Mognetti, L. Di Michele and G. Bruylants, *Langmuir*, 2019, **35**, 2002–2012.
21 M. R. W. Scheepers, L. J. van IJzendoorn and M. W. J. Prins, *Proc. Natl. Acad. Sci. U. S. A.*, 2020, **117**, 22690–22697.
22 M. Liu, A. Apriceno, M. Sipin, E. Scarpa, L. Rodriguez-Arco, A. Poma, G. Marchello, G. Battaglia and S. Angioletti-Uberti, *Nat. Commun.*, 2020, **11**, 4836.

23 M. Deserno, *Phys. Rev. E*, 2004, **69**, 031903.
24 I. Koltover, J. O. Rädler and C. R. Safinya, *Phys. Rev. Lett.*, 1999, **82**, 1991–1994.
25 B. J. Reynwar, G. Illya, V. A. Harmandaris, M. M. Müller, K. Kremer and M. Deserno, *Nature*, 2007, **447**, 461–464.
26 R. Sarfati and E. R. Dufresne, *Phys. Rev. E*, 2016, **94**, 012604.
27 C. van der Wel, A. Vahid, A. Šarić, T. Idema, D. Heinrich and D. J. Kraft, *Sci. Rep.*, 2016, **6**, 32825.
28 A. Šarić and A. Cacciuto, *Soft Matter*, 2013, **9**, 6677–6695.
29 S. Zuraw-Weston, D. A. Wood, I. K. Torres, Y. Lee, L.-S. Wang, Z. Jiang, G. R. Lázaro, S. Wang, A. A. Rodal, M. F. Hagan, V. M. Rotello and A. D. Dinsmore, *Nanoscale*, 2019, **11**, 18464–18474.
30 Y. Wang, Y. Wang, X. Zheng, É. Ducrot, J. S. Yodh, M. Weck and D. J. Pine, *Nat. Commun.*, 2015, **6**, 7253.
31 D. C. Prieve, *Adv. Colloid Interface Sci.*, 1999, **82**, 93–125.
32 J. C. Crocker and D. G. Grier, *J. Colloid Interface Sci.*, 1996, **179**, 298–310.
33 G. Volpe, T. Brettschneider, L. Helden and C. Bechinger, *Opt. Express*, 2009, **17**, 23975–23985.
34 W. B. Rogers and J. C. Crocker, *Proc. Natl. Acad. Sci. U. S. A.*, 2011, **108**, 15687–15692.
35 N. Ben-Tal, B. Honig, C. K. Bagdassarian and A. Ben-Shaul, *Biophys. J.*, 2000, **79**, 1180–1187.
36 M. F. Hagan, *J. Chem. Phys.*, 2009, **130**, 114902.
37 J. SantaLucia Jr., *Proc. Natl. Acad. Sci. U. S. A.*, 1998, **95**, 1460–1465.
38 B. Gumí-Audenis, L. Costa, L. Ferrer-Tasies, I. Ratera, N. Ventosa, F. Sanz and M. I. Giannotti, *Nanoscale*, 2018, **10**, 14763–14770.
39 D. Marsh, R. Bartucci and L. Sportelli, *Biochim. Biophys. Acta, Biomembr.*, 2003, **1615**, 33–59.
40 H. Brenner, *Chem. Eng. Sci.*, 1961, **16**, 242–251.
41 E. Evans and E. Sackmann, *J. Fluid Mech.*, 1988, **194**, 553–561.
42 P. J. Flory, *Principles of Polymer Chemistry*, Cornell University Press, Ithaca, NY, 1953.
43 D. F. Kucik, E. L. Elson and M. P. Sheetz, *Biophys. J.*, 1999, **76**, 314–322.
44 J. D. Knight, M. G. Lerner, J. G. Marcano-Velázquez, R. W. Pastor and J. Falke, *Biophys. J.*, 2010, **99**, 2879–2887.
45 P. G. Saffman and M. Delbrück, *Proc. Natl. Acad. Sci. U. S. A.*, 1975, **72**, 3111–3113.
46 N. Oppenheimer and H. Diamant, *Biophys. J.*, 2009, **96**, 3041–3049.
47 B. D. Hughes, B. A. Pailthorpe and L. R. White, *J. Fluid Mech.*, 1981, **110**, 349–372.
48 E. P. Petrov and P. Schwille, *Biophys. J.*, 2008, **94**, L41–L43.
49 A. Bunge, M. Loew, P. Pescador, A. Arbuzova, N. Brodersen, J. Kang, L. Dähne, J. Liebscher, A. Herrmann, G. Stengel and D. Huster, *J. Phys. Chem. B*, 2009, **113**, 16425–16434.
50 A. Lopez and J. Liu, *Langmuir*, 2018, **34**, 15000–15013.
51 W. Helfrich, *Z. Naturforsch. C*, 1973, **28**, 693–703.
52 H. T. McMahon and J. L. Gallop, *Nature*, 2005, **438**, 590–596.
53 A. Frost, R. Perera, A. Roux, K. Spasov, O. Destaing, E. Egelman, P. De Camilli and V. Unger, *Cell*, 2008, **132**, 807–817.
54 V. Saranathan, C. O. Osuji, S. G. J. Mochrie, H. Noh, S. Narayanan, A. Sandy, E. R. Dufresne and R. O. Prum, *Proc. Natl. Acad. Sci. U. S. A.*, 2010, **107**, 11676–11681.
55 S. Sacanna, W. T. M. Irvine, L. Rossi and D. J. Pine, *Soft Matter*, 2011, **7**, 1631–1634.
56 N. R. Markham and M. Zuker, *Nucleic Acids Res.*, 2005, **33**, W577–W581.
57 N. R. Markham and M. Zuker, in *UNAFold: Software for Nucleic Acid Folding and Hybridization*, ed. J. M. Keith, Humana Press, Totowa, NJ, 2008, pp. 3–31.

